

Spin-parity Analysis of an $\omega\pi^-$ Enhancement Seen in $\overline{B} \rightarrow D\omega\pi^-$ Decays

Abstract

We report on the observation of $B \rightarrow D\omega\pi^-$ decays. The branching ratios for D^+ and D^0 are $(0.28 \pm 0.05 \pm 0.03)\%$ and $(0.41 \pm 0.07 \pm 0.04)\%$, respectively. The $\omega\pi^-$ appears to come from the decay of a resonance of mass 1418 ± 26 MeV and width 388 ± 44 MeV, that has a J^P of 1^- .

1 Introduction

We have previously reported (CBX-0016)[1] on the reactions $\overline{B} \rightarrow D^*\omega\pi^-$, where we seen that the $\omega\pi^-$ appear to arise from the decay of a wide resonance of mass 1419 ± 33 MeV and width 382 ± 44 MeV. However the vector-vector nature of the final state allowed us to conclude only that the intrinsic angular momentum was greater than zero.

Here we study the reactions $\overline{B} \rightarrow D\omega\pi^-$, with either a $D^0 \rightarrow K^-\pi^+$ or $D^+ \rightarrow K^-\pi^+\pi^+$ decay. Observing these final states means engaging in a war with backgrounds. Using other D^0 or D^+ decays means losing that war.

We report an analysis from a data sample consisting of 9.0 fb^{-1} of integrated luminosity taken with the CLEO II and II.V detectors using the CESR e^+e^- storage ring on the peak of the $\Upsilon(4S)$ resonance and 4.4 fb^{-1} in the continuum at 60 MeV less center-of-mass energy. The sample contains 19.4 million B mesons.

2 Observation of $\overline{B} \rightarrow D\omega\pi^-$ Decays

2.1 Event selection

Track candidates are required to pass a series of cuts listed in the appendix. Photon candidates are required to be within the “good barrel region,” within 45° of the normal to the beam line.

We require that the invariant mass of the candidates lie within $\pm 2.5\sigma$ of the known D masses. The σ 's are listed in Table 1. The D^0 widths vary with the D^0 momentum, p , (units of MeV). We did not find significant differences between the CLEO II and II.V data sets.

Neutral pions are formed by selecting photon pairs that are in the good barrel region; they are required to have E9/E25 probabilities greater than 99% and not be fragments (see

Table 1: Mass Resolutions (σ) in MeV

$D^0 \rightarrow K^- \pi^+$	$D^+ \rightarrow K^- \pi^+ \pi^+$
$p \times 0.93 \times 10^{-3} + 6.0$	6.0

appendix). The photons pairs then are required to have an invariant mass within -3 and $+2.5\sigma$ of the π^0 mass. The energy and momentum of π^0 candidate is derived from mass constraint fit.

To reject continuum we require that the Fox-Wolfram moment R_2 be less than 0.3 [2].

Although we are restricting our search to ω 's, we define two $\pi^+ \pi^- \pi^0$ samples. One within 20 MeV of the known ω mass (782 MeV) and the other in either low mass or high mass sideband defined as three π mass either between 732 and 752 MeV or between 812 and 832 MeV. We also require a cut on the ω Dalitz plot, defined in CBX-0016 [1], of $r < 0.7$.

For both samples, we calculate the difference between the beam energy, E_{beam} , and the measured energy of the three particles, ΔE . The ‘‘beam constrained’’ invariant mass of the B candidates, M_B , is computed from the formula

$$M_B^2 = E_{beam}^2 - \left(\sum_i \vec{p}_i \right)^2 \quad . \quad (1)$$

To further reduce backgrounds we define

$$\chi_b^2 = \left(\frac{\Delta M_D}{\sigma(\Delta M_D)} \right)^2 + \left(\frac{\Delta M_\omega}{\sigma(\Delta M_\omega)} \right)^2 + \left(\frac{\Delta M_{\pi^0}}{\sigma(\Delta M_{\pi^0})} \right)^2 \quad , \quad (2)$$

where ΔM_D is the invariant candidate D^0 mass minus the known D^0 mass, ΔM_ω is the invariant candidate ω mass minus the known ω mass, and ΔM_{π^0} is the measured $\gamma\gamma$ invariant mass minus the known π^0 mass. The σ 's are the measurement errors. We select candidate events requiring that $\chi_b^2 < C_n$, where C_n varies for each decay D decay mode. For the $K\pi$ and $K\pi\pi$ decay modes we use $C_n = 12$, and 6, respectively. The χ_b^2 spectra for data and Monte Carlo are shown in Fig. 1.

2.2 $B^- \rightarrow D^0 \omega \pi^-$ Signal

We start with the $D^0 \rightarrow K^- \pi^+$ decay mode, for events in the ω peak. We show the candidate B mass distribution, M_B for events with the difference between the measured B energy and the beam energy, ΔE , is not centered on zero but is in the bands from -7.0 to -3.0σ and 7.0 to 3.0σ on Fig. 2(a). The ΔE resolution is 18 MeV (σ). This gives a good representation of the background in the signal region. We fit this distribution with a shape given as

$$back(r) = p_1 r \sqrt{1 - r^2} e^{-p_2(1-r^2)} \quad , \quad (3)$$

where $r = M_B/5.2895$, and the p_i are parameters given by the fit.

We next view the M_B distribution for events having ΔE within 2σ around zero in Fig. 2(b). This distribution is fit with a Gaussian signal function of width 2.7 MeV and the

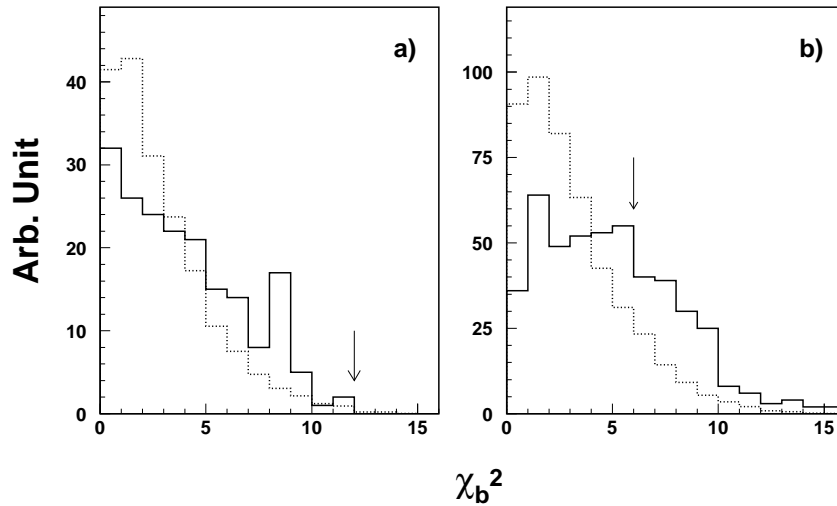


Figure 1: The χ_b^2 spectra for the final state $\bar{B} \rightarrow D\omega\pi^-$ for (a) $D^0 \rightarrow K^-\pi^+$ and (b) $D^+ \rightarrow K^-\pi^+\pi^+$. The solid line is the data, the dashed signal Monte Carlo and the arrows indicate the selected cut values. For the data we restrict ΔE to be within of 2σ zero and an M_B to be within 2σ of the known B^0 mass.

background function found above whose normalization is allowed to vary. We find 88 ± 14 events in the signal peak.

We repeat this procedure for events in the ω sidebands. We use for our χ_b^2 definition pseudo- ω masses in the sideband intervals. We show the M_B distribution for events in the ΔE sideband, defined above, and those having ΔE within 2σ around zero in Fig. 3. We find no significant signal.

2.3 $\bar{B}^0 \rightarrow D^+\omega\pi^-$ Signal

We repeat this procedure for the D^+ decay mode. We show the candidate B mass distribution, M_B for events with the difference between the measured B energy and the beam energy, ΔE , is not centered on zero but is in the bands from -7.0 to -3.0σ and 7.0 to 3.0σ on Fig. 4(a). The ΔE resolution is 18 MeV (σ). This gives a good representation of the background in the signal region. We fit this distribution with a shape given as

$$back(r) = p_1 r \sqrt{1 - r^2} e^{-p_2(1 - r^2)} \quad , \quad (4)$$

where $r = M_B/5.2895$, and the p_i are parameters given by the fit.

We next view the M_B distribution for events having ΔE within 2σ around zero in Fig. 4(b). This distribution is fit with a Gaussian signal function of width 2.7 MeV and the background function found above whose normalization is allowed to vary. We find 91 ± 18 events in the signal peak.

We repeat this procedure for events in the ω sidebands. We show the M_B distribution for both ΔE sidebands and ΔE within 2σ around zero in Fig. 5.

There is no evidence of any signal in the ω sideband plot, leading to the conclusion that the signal is associated purely with ω .

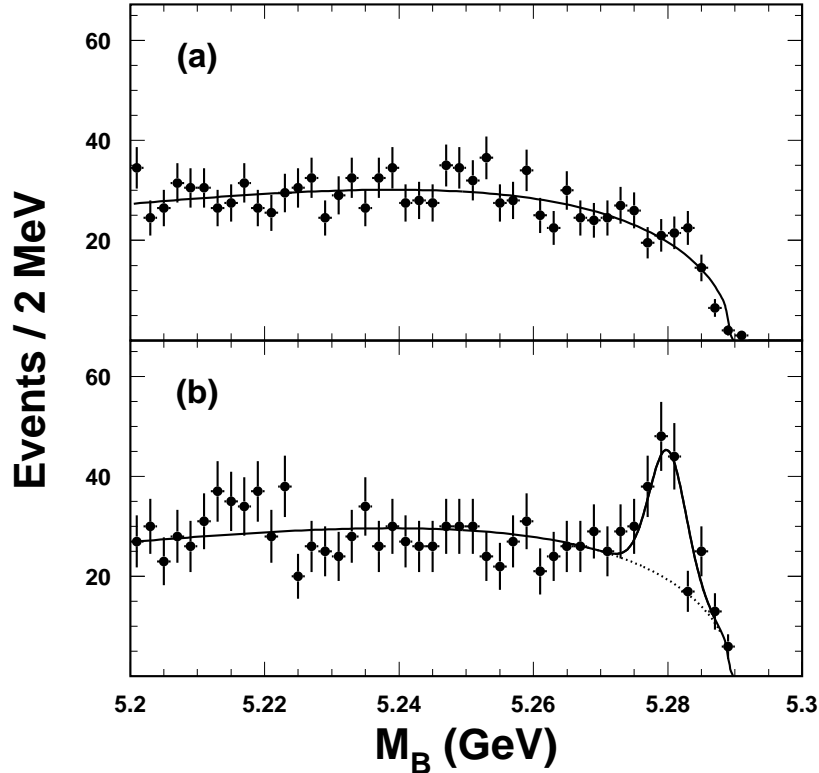


Figure 2: The B candidate mass spectra for the final state $D^0\omega\pi^-$, with $D^0 \rightarrow K^-\pi^+$. (a) for ΔE sidebands, and (b) for ΔE consistent with zero. The vertical scale in (a) was multiplied by 0.5 to facilitate comparison. The curve in (a) is a fit to the background distribution described in the text, while in (b) the shape from (a) is used with the normalization allowed to float and a signal Gaussian of width 2.7 MeV is added.

3 Branching Fractions

We can view the signal by selecting those events in the M_B signal region within 2σ of the B mass, and plotting the ΔE distribution, as shown in Fig. 6. Clear peaks near ΔE of zero are seen. (We don't use this figure any further, but include it for those who like to see it.)

We determine the branching ratios, shown in Table 2, by performing a Monte Carlo simulation of the efficiencies in the two modes. We use the current particle data group values for the relevant ω , D^+ and D^0 branching ratios of $(88.8\pm 0.7)\%$ ($\omega \rightarrow \pi^+\pi^-\pi^0$), $(9.0\pm 0.6)\%$ ($D^+ \rightarrow K^-\pi^+\pi^+$) and $(3.85\pm 0.09)\%$ ($D^0 \rightarrow K^-\pi^+$) [3]. The efficiencies listed in the Table does not include these branching ratios [4].

The systematic error arises mainly from our lack of knowledge about the tracking and π^0 efficiencies. We assign errors of $\pm 2.2\%$ on the efficiency of each charged track, and $\pm 5.4\%$ for the π^0 [5]. The error due to the background shape is evaluated in three ways. First of all, we change the background shape by varying the fitted parameters by 1σ . This results in a change of $\pm 5.0\%$. Secondly, we allow the shape, p_2 , to vary (the normalization, p_1 , was

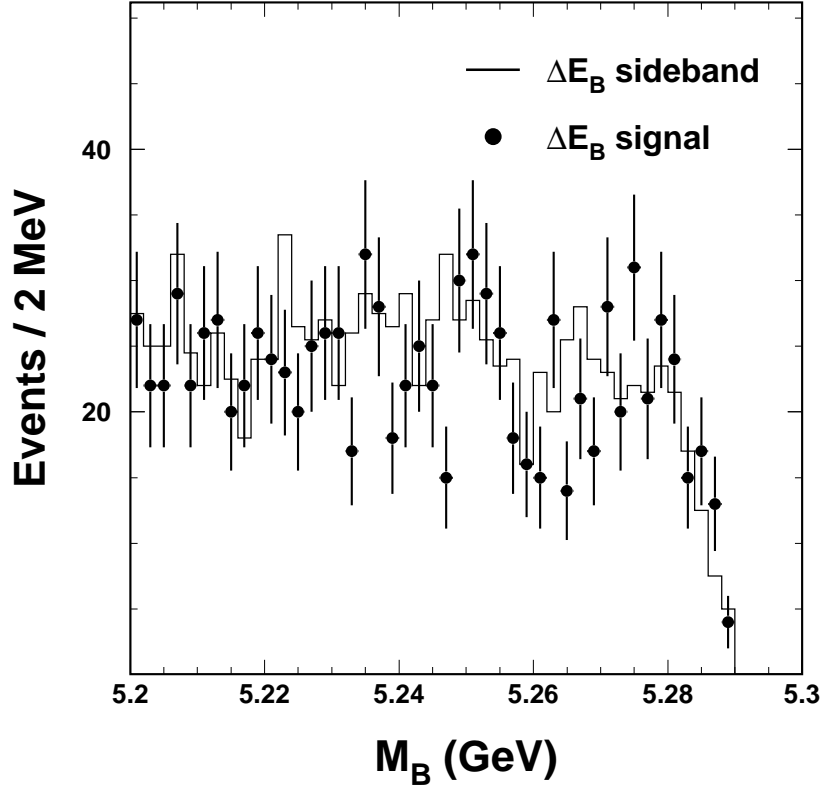


Figure 3: The B candidate mass spectra for the final state $D^0\omega\pi^-$, with $D^0 \rightarrow K^-\pi^+$ and ω sidebands (a) for ΔE sidebands and (b) for ΔE consistent with zero.

already allowed to vary). This results in 5.5% increase in the number of events. Finally, we choose a different background function

$$back'(r) = p_1 r \sqrt{1 - r^2} (1 + p_2 r + p_3 r^2 + p_4 r^3) \quad , \quad (5)$$

and repeat the fitting procedure. This results in a 1.0% decrease in the number of events. Taking a conservative estimate of the systematic error due to the background shape we arrive at $\pm 5.5\%$.

Table 2: Branching Fractions for the $D\omega\pi^-$ final state

D^0 Decay Mode	Fitted # of events	Efficiency	Branching Fraction (%)
$K^-\pi^+$	88 ± 14	0.064	$0.41 \pm 0.07 \pm 0.04$
$K^-\pi^+\pi^+$	91 ± 18	0.046	$0.28 \pm 0.05 \pm 0.03$

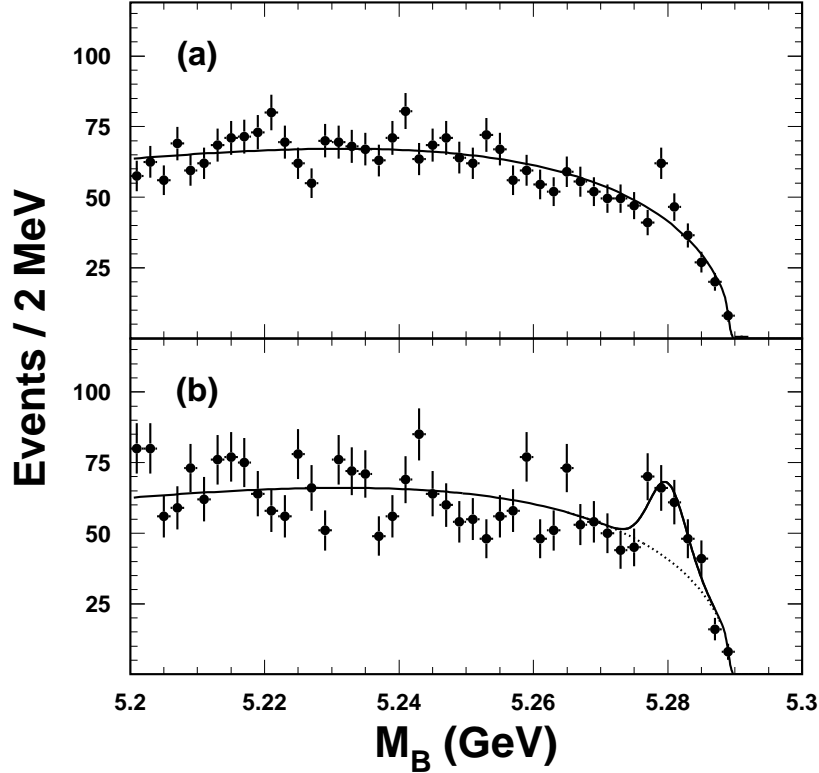


Figure 4: The B candidate mass spectra for the final state $D^+\omega\pi^-$, with $D^+ \rightarrow K^-\pi^+\pi^+$ (a) for ΔE sidebands and (b) for ΔE consistent with zero. The vertical scale in (a) was multiplied by 0.5 to facilitate comparison. The curve in (a) is a fit to the background distribution described in the text, while in (b) the shape from (a) is used with the normalization allowed to float and a signal Gaussian of width 2.7 MeV is added.

4 The $\omega\pi^-$ System

For all subsequent discussions we add the D^0 and D^+ final states together.

We select sample of ω 's in the $\pi^+\pi^-\pi^0$ mass window of 782 ± 20 MeV with Dalitz plot selection of $r < 0.7$ (see CBX-0016 for details).

In Fig. 7 we show the $\omega\pi^-$ mass spectrum in the left-side plot. The solid histogram shows events from the lower M_B sideband region (5.203 - 5.257 GeV) suitably normalized. The dotted histogram shows the background estimate from the ΔE sidebands, again normalized. In the signal distribution there is a wide structure around 1.4 GeV, that is inconsistent with background. We re-determine the $\omega\pi^-$ mass distribution by fitting the M_B distribution in bins of $\omega\pi^-$ mass, and this is shown on the right-side. Fitting to a Breit-Wigner function, we find a peak value of 1415 ± 43 MeV and a width of 419 ± 110 MeV. Since the $\omega\pi^-$ mass distribution is obtained by fitting the M_B distribution, systematic errors in the Breit-Wigner fit are negligible. However, it should be kept in mind that this particular signal shape is

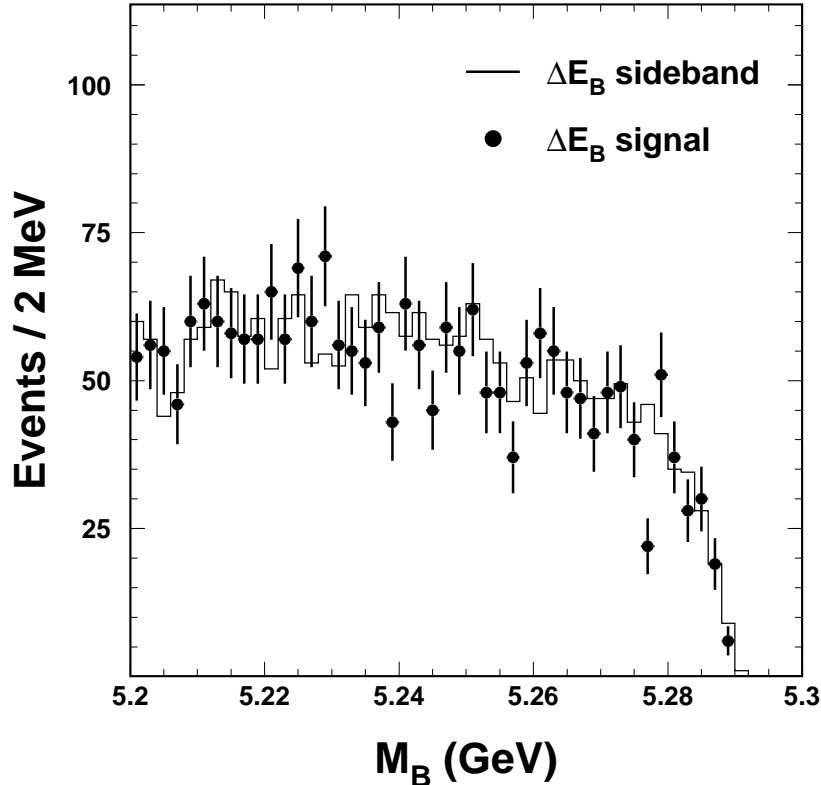


Figure 5: The B candidate mass spectra for the final state $D^+\omega\pi^-$, with $D^+ \rightarrow K^-\pi^+\pi^+$ and ω sidebands (a) for ΔE sidebands and (b) for ΔE consistent with zero.

assumed to be correct. Other resonant or non-resonant contributions could affect the mass and width.

This structure is almost identical to the one we observed in $\bar{B} \rightarrow D^*\omega\pi^-$ decays in CBX-0016, that we call the A^- .

5 Angular Distributions

We may be able to determine the spin and parity of the A particle by studying the angular distributions characterizing its decay products. The decay chain that we are considering is $B \rightarrow A D$; $A \rightarrow \omega\pi$ and $\omega \rightarrow \pi^+\pi^-\pi^0$. The helicity formalism[6], [7], [8] is generally used in the analysis of these sequential decays. This formalism is well suited to relativistic problems involving particles with spin \vec{S} and momentum \vec{p} because the helicity operator $h = \vec{S} \cdot \vec{p}$ is invariant under both rotations and boosts along \hat{p} .

There are two relevant reference frames. The first one, that we will define $x_A y_A z_A$ is the rest frame of the A particle, with the \hat{z}_A axis pointing in the A direction of motion in the B rest frame. The second one, $x_\omega y_\omega z_\omega$, is related to $x_A y_A z_A$ by the rotation through 3 Euler angles $\phi_A, \theta_A, -\phi_A$, as shown in Fig. 8. The angle ϕ_A defines the orientation of the plane

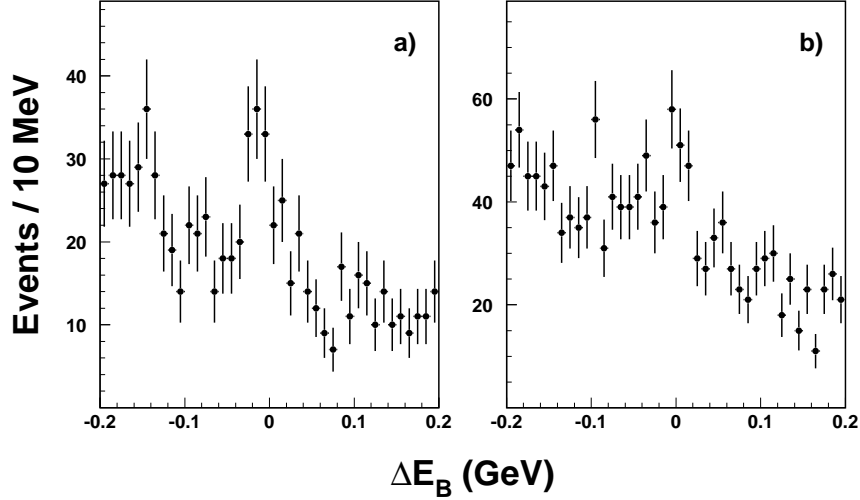


Figure 6: The ΔE spectrum for the final state $D\omega\pi^-$ restricted to combinations within 2σ of the B mass with (a) $D^0 \rightarrow K^-\pi^+$ and (b) $D^+ \rightarrow K^-\pi^+\pi^+$.

containing the ω direction in the A rest frame and the \hat{z}_A axis with respect to the $\hat{x}_A - \hat{z}_A$ plane. The \hat{x}_A direction is arbitrary. The angles θ_ω and ϕ_ω define the orientation of the ω decay plane in the ω rest frame. Note that the A decay plane has an azimuthal angle ϕ_A both in the $x_A y_A z_A$ and in the $x_\omega y_\omega z_\omega$ references. As the angle ϕ_A is arbitrary, the only angle that has a physical meaning is $\chi = \phi_A - \phi_\omega$, the opening angle between the A decay plane and the ω decay plane.

Both the B meson and the D meson are pseudoscalar, therefore their helicity is 0. Thus A will be longitudinally polarized independently of its spin. In order to calculate the decay amplitude for this process, we need to sum over the ω helicity states:

$$\mathcal{A} = \sum_{\lambda_\omega} D_{0\lambda_\omega}^{*J_A}(\phi_A, \theta_A, -\phi_A) D_{\lambda_\omega 0}^{*1}(\phi_\omega, \theta_\omega, -\phi_\omega) B_{\lambda_\omega 0}, \quad (6)$$

here $D_{\lambda_\omega}^{*1}(\phi_A, \theta_A, -\phi_A)$ is the rotation matrix that relates the $x_A y_A z_A$ and the $x_\omega y_\omega z_\omega$ frames and $D_{\lambda_\omega}^{*1}(\phi_\omega, \theta_\omega, -\phi_\omega)$ is the rotation matrix relating the $x_\omega y_\omega z_\omega$ and the direction of the normal to the ω decay plane $\hat{n}(\theta_\omega, \phi_\omega)$.

In general, there are three helicity amplitudes that contribute to this decay: B_{10} and B_{-10} , corresponding to a transverse ω polarization, and B_{00} , corresponding to a longitudinal ω polarization. This expression can be simplified by observing that $A \rightarrow \omega\pi$ is a strong decay and thus it conserves parity. Thus, the helicity amplitudes are related by the equation:

$$B_{10} = (-1)^{1-S(A)} \eta_A \eta_\omega \eta_\pi B_{-10}, \quad (7)$$

$$B_{00} = (-1)^{1-S(A)} \eta_A \eta_\omega \eta_\pi B_{00}. \quad (8)$$

where $S(A)$ is the spin of particle A and η_A, η_ω and η_π represent the intrinsic parity of the decaying particle and its decay products respectively.

Eq. 7 relates the two transverse helicity amplitudes, while Eq. 8 forbids the presence of a longitudinal component under certain conditions. For example, if A is a 1^- object, ω

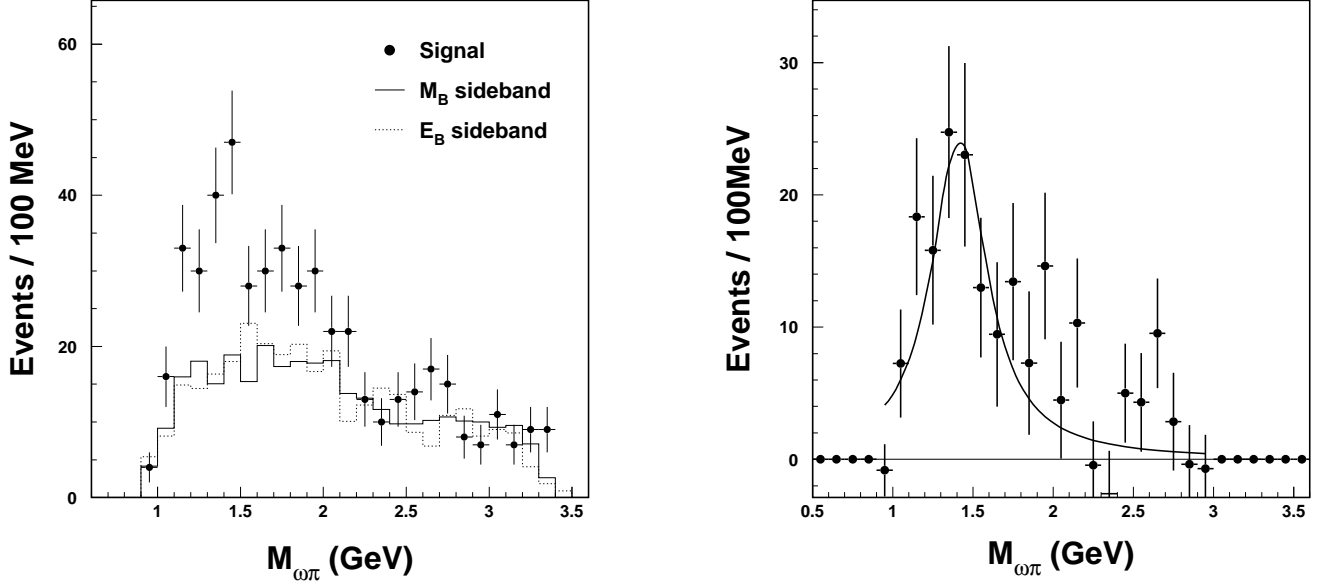


Figure 7: The invariant mass spectra of $\omega\pi^-$ for the final state $D\omega\pi^-$ for both D decay modes. (left) The solid histogram is the background estimate from the M_B lower sideband and the dashed histogram is from the ΔE sidebands; both are normalized to the fitted number of background events. (right) The mass spectrum determined from fitting the M_B distribution and fit to a Breit-Wigner function.

has transverse polarization and $B_{-10} = -B_{10}$. When the sign in Eqs. 7-8 is positive, two parameters determined by the hadronic matrix element affect the angular distribution and thus we cannot fully determine it only on the basis of our assumptions on the A spin parity. We have carried out the calculation of the predicted angular distributions including spin assignment for A up to 2. The predicted angular distributions are summarized in Table 3.

The statistical accuracy of our data sample is not sufficient to do a simultaneous fit of the joint angular distributions shown above. Thus only the projections along the θ_A , θ_ω and χ are fitted, integrating out the remaining degrees of freedom. Table 4, gives the analytical form for these projections.

We determine the projections of these angular distributions by fitting the M_B distribution

Table 3: Differential angular distributions (modulo a proportionality constant) predicted for different spin assignments.

J^η	$d\sigma/d\cos\theta_A d\cos\theta_\omega d\chi$
0^-	$ B_{00} ^2 \cos^2 \theta_\omega$
1^-	$ B_{10} ^2 \sin^2 \theta_A \sin^2 \theta_\omega \sin^2 \chi$
1^+	$ B_{10} ^2 \sin^2 \theta_A \sin^2 \theta_\omega^2 \cos^2 \chi + B_{00} ^2 \cos^2 \theta_A \cos^2 \theta_\omega - 1/2 \text{Re}(B_{10} B_{00}^*) \sin 2\theta_A \sin 2\theta_\omega \cos \chi$
2^-	$3 B_{10} ^2 \sin^2 2\theta_A \sin^2 \theta_\omega \cos^2 \chi + B_{00} ^2 (3 \cos^2 \theta_A - 1)^2 \cos^2 \theta_\omega$
	$-\sqrt{3} \text{Re}(B_{10} B_{00}^*) \sin 2\theta_A (3 \cos^2 \theta_A - 1) \sin 2\theta_\omega \cos \chi$
2^+	$3/4 B_{10} ^2 \sin^2 2\theta_A \sin^2 \theta_\omega \sin^2 \chi$

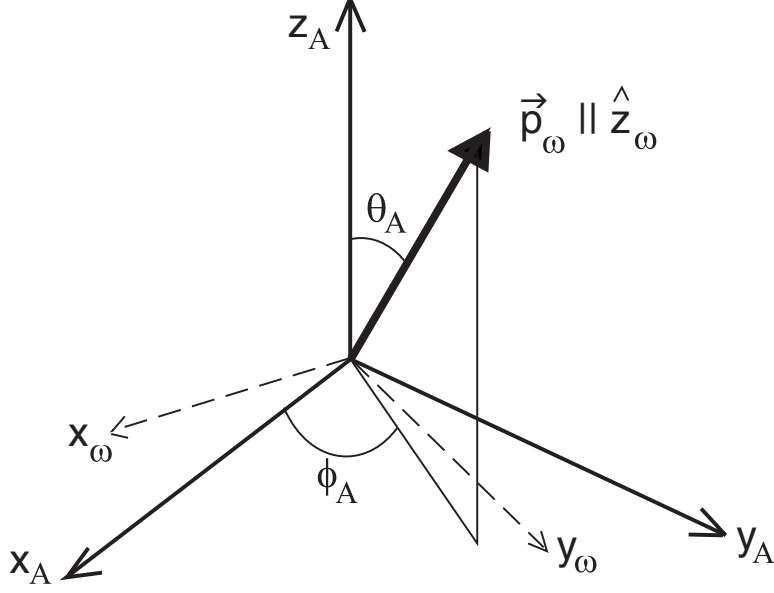


Figure 8: Relationship between the A rest frame $x_A y_A z_A$ and the ω rest frame $x_\omega y_\omega z_\omega$. x_A and x_ω lie in the same plane.

Table 4: Projection of the angular distributions along the $\cos \theta_A$, $\cos \theta_\omega$ and χ axes.

J^η	$d\sigma/d \cos \theta_A$	$d\sigma/d \cos \theta_\omega$	$d\sigma/d \chi$
0^-	$\frac{4\pi}{3} B_{00} ^2$	$4\pi B_{00} ^2 \cos^2 \theta_\omega$	$4/3 B_{00} ^2$
1^-	$\frac{4\pi}{3} B_{10} ^2 \sin^2 \theta_A$	$\frac{4\pi}{3} B_{10} ^2 \sin^2 \theta_\omega$	$\frac{8}{9} B_{10} ^2 \sin^2 \chi$
1^+	$\frac{4\pi}{3}(B_{10} ^2 \sin^2 \theta_A + B_{00} ^2 \cos^2 \theta_A)$	$\frac{4\pi}{3}(B_{10} ^2 \sin^2 \theta_\omega + B_{00} ^2 \cos^2 \theta_\omega)$	$\frac{4}{9}(4 B_{10} ^2 \cos^2 \chi + B_{00} ^2)$
2^-	$\frac{4\pi}{3}(3 B_{10} ^2 \sin^2 2\theta_A + B_{00} ^2(3 \cos^2 \theta_A - 1)^2)$	$\frac{16\pi}{5}(B_{10} ^2 \sin^2 \theta_\omega + B_{00} ^2 \cos^2 \theta_\omega)$	$4 B_{10} ^2 \cos^2 \chi + B_{00} ^2$
2^+	$\pi B_{10} ^2 \sin^2 2\theta_A$	$\frac{4\pi}{5} B_{10} ^2 \sin^2 \theta_\omega$	$\frac{16}{15} B_{10} ^2 \sin^2 \chi$

in as a function of the various angular quantities $\cos \theta_A$, $\cos \theta_\omega$, χ . We restrict the $\omega\pi^-$ mass range to be between 1.1 and 1.7 GeV, a total of 104 events. In order to fit the angular distribution with theoretical expectations, we must correct the data for acceptances. We determine the acceptance correction by comparing the Monte Carlo generated angular distributions with the reconstructed distributions. The angular dependent efficiencies are shown in Fig. 9.

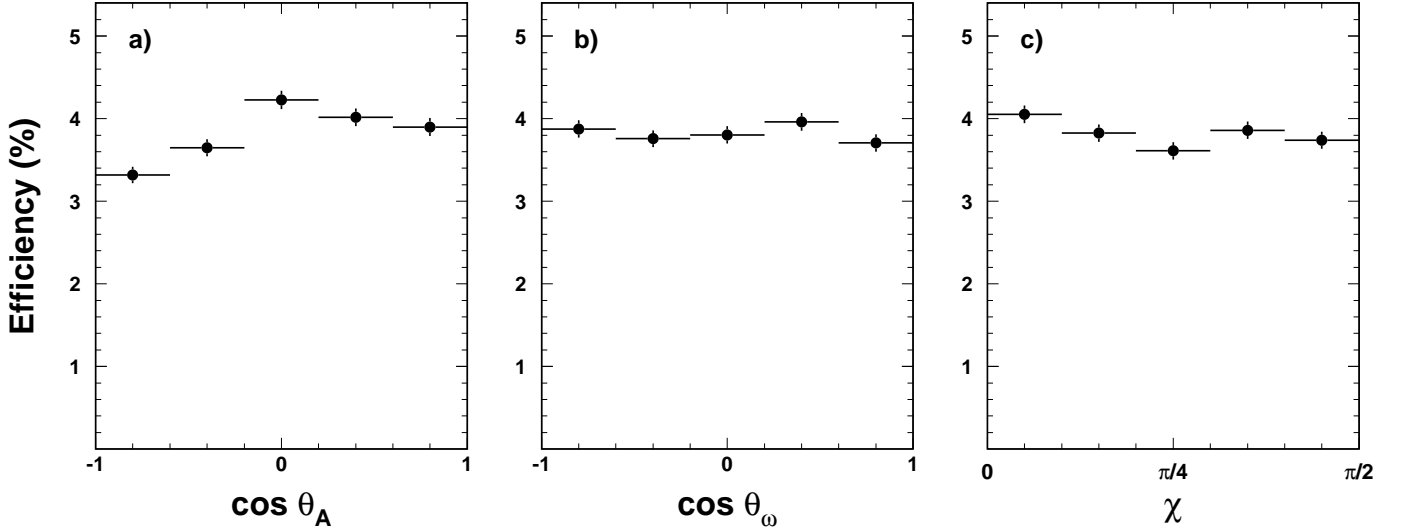


Figure 9: Reconstruction efficiency dependence on (a) $\cos \theta_A$, (b) $\cos \theta_\omega$, and (c) χ .

The corrected angular distributions are shown in Fig. 10. The data are fit to the expectations for the various J^P assignments. For the 0^- , 1^- and 2^+ assignments, the curves have a fixed shape. For the 1^+ and 2^- assignments we let the ratio between the longitudinal and transverse amplitudes vary to best fit the data. We notice that the ω polarization is very clearly transverse ($\sin^2 \theta_\omega$) and that infers a 1^- or 2^+ assignment.

We list in Table 5 the $\chi^2/ndof$ for the different J^P assignments. The 1^- assignment is preferred, having a $\chi^2/ndof$ of 1.7. The other assignments are clearly ruled out. The probability that we have a correct solution and $\chi^2/ndof$ is 1.7 or greater is 3.8% [9].

Table 5: The χ^2 of angular fits

	0^-	1^+	1^-	2^+	2^-
$\chi^2/ndof$	7.0	4.5	1.7	3.2	5.3
probability	1.9×10^{-15}	3.3×10^{-8}	3.8%	2.7×10^{-5}	3.3×10^{-10}

6 Conclusions

The A^- is most likely the elusive ρ' [10]. Combining with our previous measurements in the $D^*\omega\pi^-$ final states we determine a value of the mass of 1418 ± 26 MeV and the width of 388 ± 41 MeV. These are by far the most accurate and least model dependent measurements of the ρ' parameters.

We have made the first statistically significant observations of two hadronic B decays: $\overline{B}^0 \rightarrow D^+\omega\pi^-$, and $B^- \rightarrow D^0\omega\pi^-$. The branching fractions are $(0.28\pm 0.05\pm 0.03)\%$ and $(0.41\pm 0.07\pm 0.04)\%$, respectively. These are similar to the corresponding D^* final states, a result not unexpected in the factorization assumption.

From the $D\omega\pi^-$ final states we determine the mass and width to be 1415 ± 43 MeV and 419 ± 110 MeV. Combining with the $D^*\omega\pi^-$ results we find 1418 ± 26 MeV and 388 ± 41 MeV.

References

- [1] R. Ayad, S. Stone and J. C. Wang, CBX 00-16.
- [2] G. Fox and S. Wolfram, Phys. Rev. Lett. **23**, 1581 (1978).
- [3] C. Caso *et al.*, The European Physical Journal **C3** (1998) 1.
- [4] We assume that $\omega\pi$ is in a 1^- final state. The difference between the 1^- efficiency and flat assumption is less than 2
- [5] S. Schuh and S. Stone, CBX 00-7.
- [6] M. Jacob and G.C. Wick, *Ann. Phys. (N.Y.)* **7** (1959) 404.
- [7] J. D. Jackson, in *High Energy Physics, Les Houches, 1965*, Gordon and Breach, NY (1966).
- [8] M.L. Perl, *High Energy Hadron Physics*, Wiley, NY (1974).
- [9] We allowed a systematic error of 5.5% on the number of events in each angular bin resulting possibly from the fitting procedure to the M_B spectrum. This changed the probability of χ^2 for the 1^- case to 3.9% from 3.8%, and negligible changes in the other cases.
- [10] A. B. Clegg and A. Donnachie, Z. Phys. **C 62**, 455 (1994).

7 Appendix: Details of Selection Requirements

7.1 Charged Track Cuts

Tracks must pass Trackman.

Kincd must be zero.

These are the only cuts for the slow pion from the D^{*+}

For other tracks above 250 MeV we require $dbcd < 0.005$ and $|z0cd-zvptx| < 0.03$
If the track is below 250 MeV we require $dbcd < 0.01$ and $|z0cd-zvptx| < 0.05$

7.2 Particle Identification Cuts

For tracks above 900 MeV/c we do not require any particle identification.

For tracks below 900 MeV/c we require 3σ consistency, if the information is present ($iqaldi > 0$).

7.3 Photon Selection

We use XBAL.

We require that the bump energy be > 30 MeV in the good barrel region, $\cos \theta < 0.707$.

The E9/E25 distribution must look like a photon, $e925u > c92501$.

Photon candidates must not be shower fragments, $ibstop=0$.

Finally, the angle with closest charged track must be $> 20^\circ$.

7.4 π^0 Selection

Photons are selected from bumps. If both bumps belong to a multi-bump region, they must come from the same region.

We require that the diphoton invariant mass be between -3.0 to $+2.5\sigma$, where $\sigma = 5.46$ MeV.

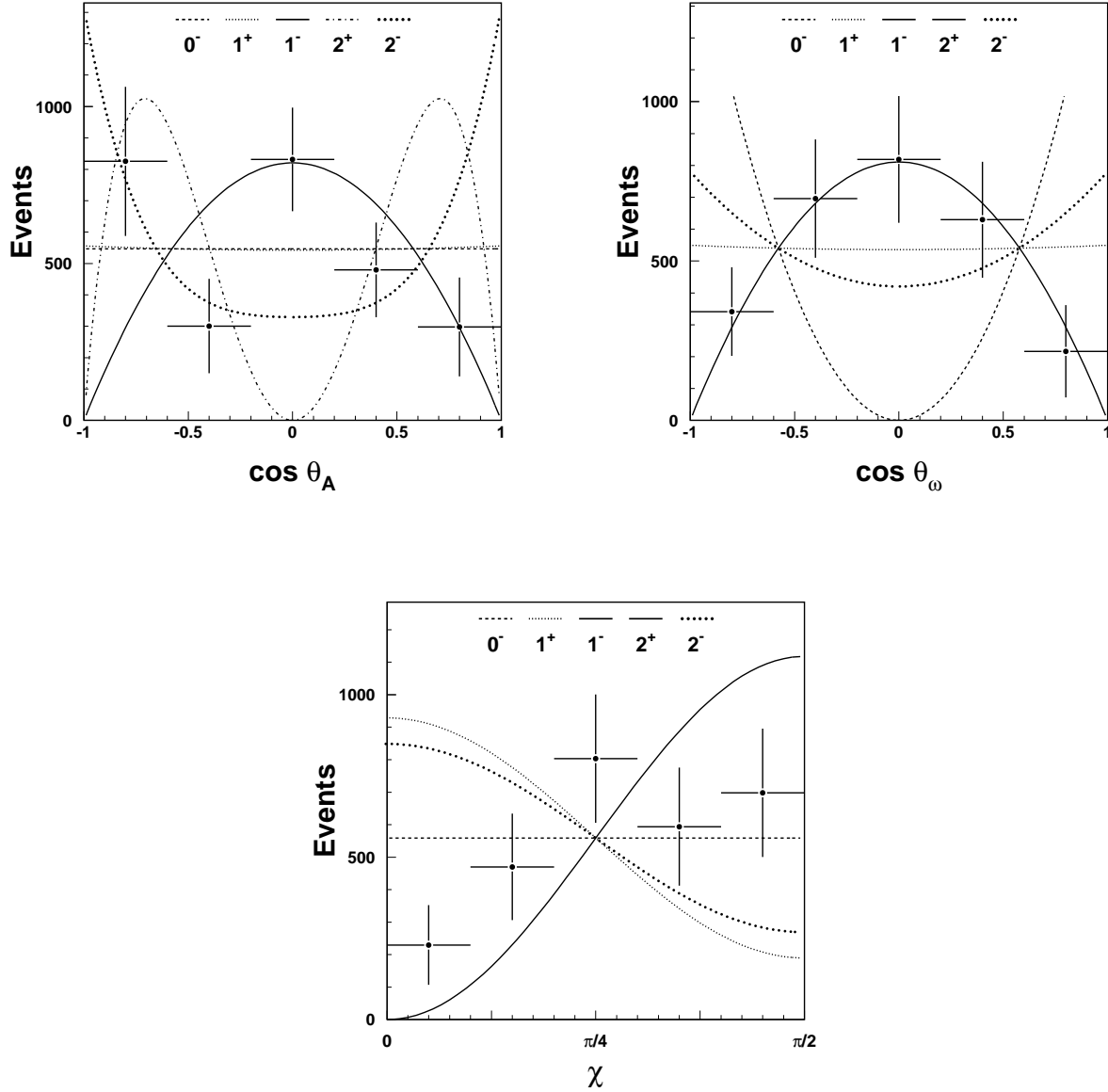


Figure 10: The angular distribution of θ_A (top-left), θ_ω (top-right) and χ (bottom). The curves show the best fits to the data for for different J^P assignments. (The 0^- and 1^+ are almost indistinguishable in $\cos \theta_A$, while the 1^- and 2^+ are indistinguishable in $\cos \theta_\omega$ and χ).